IEEE Access
Multidisciplinary | Rapid Review | Open Access Journal

Received 8 August 2023, accepted 21 August 2023, date of publication 24 August 2023, date of current version 8 September 2023.

Digital Object Identifier 10.1109/ACCESS.2023.3308293

RESEARCH ARTICLE

Collaborative Optimization Allocation of Grid-Forming and Grid-Following Reactive Power Resources Considering Auxiliary Equipment Services

SHIWEI XUE[1,2], SIMING ZENG[1], QINGQUAN JIA[2], XUEKAI HU[1], PENG LUO[1], JIFENG LIANG[1], LEI WANG[1], AND WEN ZHOU[1]

[1]State Grid Hebei Electric Power Research Institute, Shijiazhuang, Hebei 050021, China
[2]Key Laboratory of Power Electronics for Energy Conservation and Motor Drive of Hebei Province, Yanshan University, Qinhuangdao, Hebei 066004, China

Corresponding author: Shiwei Xue (xueshiweihao@163.com)

This work was supported by the National Natural Science Foundation of China under Grant 51877186.

ABSTRACT The large-scale integration of high-penetration distributed photovoltaic systems into distribution networks can result in significant grid voltage fluctuations within a short period. However, centralized regulation instructions for passive/reactive compensation, by themselves, are insufficient for effectively suppressing these fluctuations. Thus, this study used the grid-forming and grid-following control characteristics of modern power electronic inverters to propose an optimal allocation strategy for reactive power compensation equipment. This strategy aimed to address the insufficient proactive support capacity in the reactive power equipment used to suppress short-time grid voltage fluctuations. After establishing uncertain operation scenarios for the distribution network, we analyzed the respective multi-timescale behavioral characteristics of traditional, grid-forming, and grid-following reactive power compensation devices. The primary and auxiliary objectives were to minimize the investment cost of the special equipment and voltage deviation of the entire network, respectively. To achieve these objectives, we established a collaborative optimal allocation model for grid-forming and grid-following reactive power equipment. A multi-timescale cooperative allocation strategy was proposed to decompose the total reactive power demand curves at the equipment installation nodes into reactive power curves for different response levels and then collaboratively allocate the multiple devices. A comparative analysis of the three schemes in IEEE 33-node and 69-node systems shows that the proposed strategy guarantees lower overall network voltages while reducing the cost by at least 20% compared to those of other schemes.

INDEX TERMS Collaborative optimization allocation, photovoltaic inverter, multi-time scale, grid-forming control, optimal reactive power.

I. INTRODUCTION

A. MOTIVATION

"Building a new power system with a focus on renewable energy" is one of the essential measures established to achieve China's goals of carbon neutrality and peak carbon dioxide emissions [1], [2]. The National Energy Administration of China has also released the "Fourteenth Five-Year Plan for Science and Technology Innovation in the Energy Sector." The plan aims to make significant advancements in active support and control technologies to integrate renewable power generation with grid voltage control, thereby smoothly integrating large amounts of renewable energy into the grid.

The continuous integration of large-scale photovoltaic (PV) power-generation networks into the grid causes a drop in the short-circuit capacity of the system, decreasing the voltage support capacity. This exasperates the system overvoltage

The associate editor coordinating the review of this manuscript and approving it for publication was Ehab Elsayed Elattar.

This work is licensed under a Creative Commons Attribution-NonCommercial-NoDerivatives 4.0 License.
For more information, see https://creativecommons.org/licenses/by-nc-nd/4.0/

problem. In turn, this may cause the tolerance level of the new energy equipment to be exceeded and large-scale off-grid equipment to become damaged [3], [4], [5]. It is difficult to maintain the stable and reliable operation of a power grid using only traditional reactive power compensation equipment. However, utilizing the controllable and diverse functional characteristics of modern power electronic equipment can greatly improve the grid's power supply level [6], [7], [8]. In this context, distribution networks with high-penetration PV systems experience fast and slow fluctuation changes in voltage; however, the special reactive power equipment have different time-varying behaviors [9], [10]. As a result, various pressing issues have arisen. These concern, e.g., the allocation of installation locations and capacity of special reactive equipment, reducing investment costs, comprehensively improving the power supply of the distribution network, and achieving the dual goals of improving the economy and providing effective reactive power compensation.

B. SUMMARY OF CHALLENGES OF PREVIOUS STUDIES

Rationally allocating the capacities of modern power electronic reactive power compensation equipment and harnessing their performance advantages can effectively suppress system voltage fluctuations, thereby improving the power supply quality of a grid. In [11], a modified salp swarm optimization algorithm was used to configure the optimal position and capacity of a static synchronous series compensator. In [12], the location and capacity of a static var compensator (SVC) was optimized while considering the constant and adjustable characteristics of the load, with the objective of minimizing the network loss and voltage deviations. In other studies [13], [14], [15], [16], the entire network voltage deviation, network loss, and reactive power compensation cost indexes have been considered. In addition, optimization algorithms such as whale-hunting algorithm and particle swarm algorithm have been used to optimize the location and capacity of a static synchronous compensator or static var generator (SVG). However, the aforementioned studies [11], [12], [13], [14], [15], [16] considered different optimization objectives for the optimization of the configuration of a single dedicated equipment, i.e., without reflecting the differences between the dedicated reactive equipment.

The synergistic allocation of different dedicated equipment can further improve system operations. Other recent studies [17], [18] considered the uncertainty in a distributed generation output. The location and capacity of the SVC and a thyristor-controlled series compensator were optimized to minimize network power losses, voltage deviations, and system operating costs. In [19], the overlapping governance partitions of reactive power resources were identified and subdivided. Then, the voltage governance effectiveness was analyzed to optimize the configuration of the dedicated equipment. However, modern power electronic devices are generally expensive despite their multifunctionality and controllability. By contrast, traditional mechanical throwing and cutting equipment are cheaper. An optimal configuration combined with those types of equipment can reduce the investment cost of the dedicated equipment [20], [21]. In [20], a golden ratio optimization algorithm was adopted to determine the optimal and simultaneous allocation of capacitors and distribution static compensators. The aim was to minimize the power loss cost, reactive investment cost, and voltage deviations in a grid. In [21], a two-stage allocation method was proposed for coordinated reactive power optimization to minimize the equipment investment cost and voltage deviations. The capacitors were prioritized first, followed by the SVGs.

Using PV inverters to enhance the reactive power optimization can further reduce the costs of dedicated reactive power equipment configurations [22], [23], [24], [25]. In [22] and [23], the installation locations and capacities of multiple types of distributed generation and capacitors were optimized based on the adjustable power factor characteristics of the distributed generation, distributed power uncertainty, and demand response plans. In [24], the authors considered the reactive power capabilities of PV inverters in a distribution network. An optimization model was established to enhance the voltage and minimize the investment cost. Various constraints were employed, such as a voltage violation in a probabilistic form. A probabilistic approach was used to optimize configurations of SVGs and on-load regulators. In [25], the authors considered the voltage auxiliary service function of distributed generation grid-connected inverters and configured an SVG and voltage-detecting active power filters with known auxiliary equipment configurations. In general, the methods employed in the above studies [17], [18], [19], [20], [21], [22], [23], [24], [25] have reduced the configuration cost and number of dedicated reactive power equipment. However, these studies only considered the differences in the adjustable capacity steps and costs of power electronics or capacitors. The fast-response capabilities and active-reactive-voltage support of the power electronics were ignored. Moreover, the aforementioned studies largely disregarded the resilience of the distribution system. For example, they optimized equipment configurations based on typical operational scenarios (or all scenarios). This could lead to excessive allocations of resources and increased investment costs.

Incorporating chance constraints into planning models can ensure steady system operation while further reducing investment costs. In [26] and [27], a distributionally robust chance-constrained method was employed to address a conservation voltage reduction issue in distribution networks. Nevertheless, the method predominantly focused on mitigating the system risks arising from uncertainties in load- and generation-forecasting errors during optimization. Additionally, the computations involved were rather intricate.

In summary, because distributed power sources have large-scale access to a distribution network, the grid voltage significantly fluctuates within a short period of time. This makes it difficult for reactive equipment to effectively

suppress the real-time fluctuations of the grid voltage when relying only on centralized regulation and control instructions for passive-reactive power compensation. Most existing studies on optimal reactive power allocation employ reactive power responses of dedicated or part-time equipment to passively support the grid voltage. By contrast, such studies rarely consider actively supporting the grid voltage based on network control of the reactive power equipment. This results in insufficient capacities in the equipment used to suppress grid voltage fluctuations. As such, the performance(s) of the reactive power equipment cannot be fully utilized.

C. CONTRIBUTIONS AND ORGANIZATION

This study aims to consider the reactive power compensation functions of grid-forming (GFM) and grid-following (GFL) auxiliary and dedicated equipment. It also aims to reduce the cost of the dedicated equipment configuration while improving the network voltage operation level.

The main contributions of this study are as follows.

- A topology-based approach is used to change the inverter connection for providing the GFM control conditions of the PV inverter cluster, allowing the local response to be used for auxiliary grid voltage regulation services.
- Collaboration and control of multiple equipment is performed to facilitate voltage regulation in the grid according to the fast/slow characteristics of the reactive power equipment.
- A chance constraint is used to address grid uncertainty operation scenarios. A two-layer optimization allocation model is established to ensure economy and enhance grid voltage operations.

The rest of this paper is organized as follows. Section II discusses the establishment of the distribution network operation scenario through PV and load modeling in Section II. Section III provides the GFM control conditions for actively supporting the grid voltage for a distributed PV (DPV) inverter cluster. Section IV presents a two-layer allocation model for GFM and GFL reactive power resources. Sections V and VI analyze the results from case studies on IEEE 33-node systems and IEEE 69-node systems, respectively. Finally, Section VII draws the main conclusions.

II. UNCERTAIN OPERATION SCENARIOS FOR DISTRIBUTION NETWORK

Due to the high construction and operational requirements of wind power plants, wind power is currently mostly used in large power plants, while small-capacity wind power generation is less prevalent in distribution networks. Therefore, this section considers the load of the distribution network node and DPV power curves. Referring to the method in [28], the source-load power states are divided and a Markov chain principle is used to establish the connection between the different power states. Subsequently, the Gaussian and Beta distributions are combined to generate the source-load power.

A. MARKOV CHAIN PRINCIPLE FOR STATE QUANTITY OF DISTRIBUTION NETWORK

The Markov chain principle describes the state transitions of a stochastic process. The fundamental concept is that the current state only depends on the previous state and is independent of earlier states. Markov chains are extensively applied in common domains such as automatic control and optimization, prediction, information technology, and cloud/fog computing [29], [30]. In this study, the behavioral states of the PV output and load are also considered as a type of stochastic process, exhibiting a certain degree of temporal correlation. The Markov chain theory can accurately describe the evolution processes of such states. Compared to other methods, the advantage of using Markov chains lies in their ability to provide more accurate state transition probabilities while having certain advantages in terms of computational complexity. Hence, this study uses the Markov chain to represent the behavioral state changes of the PV output and load in the distribution network. The changes in the station area power consumption behaviors and PV power output are in time series. The Markov chain is used to discretize a continuum of power into distinct states to capture the power state changes in the PV equipment and station area in the distribution network. Subsequently, the station area load historical operation and PV data are used to establish a correlation relationship between the operation states and reflect the probabilistic transfer relationship(s) of the states.

Supposing that the state quantity of the distribution network is $s_{s,c}$ at a time t and shifts to $s_{s,l}$ at the next instant, the conditional probability of shifting is recorded as $p^1_{s,c,l}(t) = p_{s,c,l}(t)$, also known as the Markov shift probability. The station power consumption time and PV output time are divided into t_{ti} and t_{pvti} periods, respectively. The state transfer situation in each time period is counted to establish the system state transfer probability matrix, as follows:

$$\boldsymbol{P}(t) = \boldsymbol{P}_c(t) = \begin{bmatrix} p_{11}(t) & p_{12}(t) & \cdots & p_{1N_s}(t) \\ p_{21}(t) & p_{22}(t) & \cdots & p_{2N_s}(t) \\ \vdots & \vdots & \vdots & \vdots \\ p_{N_s1}(t) & p_{N_s2}(t) & \cdots & p_{N_sN_s}(t) \end{bmatrix}, \quad (1)$$

where N_s is the total number of load or PV output behavior states and t is the moment.

Additionally, assuming that the probability distribution of the current state at a certain moment and transfer matrix are known, the probability distribution of the system state at the next moment is determined using (2) as follows:

$$\boldsymbol{P}_s(t+1) = \boldsymbol{P}_s(t)\boldsymbol{P}(t) = \left\{p_{s,1}(t+1), \cdots, p_{s,N_s}(t+1)\right\} \quad (2)$$

where $\boldsymbol{P}_s(t) = \left\{p_{s,1}(t), p_{s,2}(t), \cdots, p_{s,N_s}(t)\right\}$, and $p_{s,s_{s,c}}(t)$ is the probability that the system is in the state $s_{s,c}$ at a moment t. For current or past states that have occurred, $p_{s,s_{s,c}}(t) = 1$ or 0, indicating that the initial state is already a deterministic event.

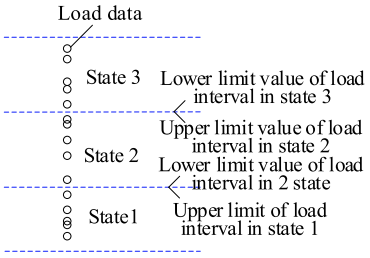

FIGURE 1. Schematic of the state division.

By setting the states $s_{s,c} = f_s(p_{s_{s,c}})$ and $f_s(x)$ as the state mapping functions, the random state at the next moment can be obtained based on the state probability outlined in (3) [28].

$$s_{s,c}(t+1) = \underset{0 \le s_{s,c} \le N_s}{f_s} (p_{s,s_{s,c}}(t+1)) \tag{3}$$

B. POWER CONSUMPTION STATE MODELING OF DISTRIBUTION NETWORK STATION AREA

The normal distribution can sufficiently characterize the uncertainty in the electricity load consumption. The probability model parameters are influenced by the electricity load consumption state [31], [32]. The variability in the electricity load consumption at different station moments is large. In this study, the stations at each moment on the distribution network node are divided into multiple electricity consumption states, each corresponding to a normal distribution. Multiple normal distributions are used to characterize the uncertainty in the electricity consumption. The maximum and minimum historical values at each moment are equated by dividing the load into multiple electricity consumption states, as shown in Fig. 1.

The total number of load power state divisions is defined as K. The power probability density of each power state corresponds to a normal distribution. Therefore, the probability density function of the kth power state of the load can be established based on (4) as follows:

$$\begin{aligned} f_J(s_L|\mu_k, \sigma_k) &= \phi(s_L|\mu_k, \sigma_k) \\ &= \frac{1}{\sqrt{2\pi}\sigma_k} \exp[-\frac{(s_L - \mu_k)^2}{2\sigma_k^2}], \end{aligned} \tag{4}$$

where s_L is the apparent power of the nodal load. μ_k and σ_k are the mean and standard deviation of the k normal distribution, respectively.

Because the different nodes in many distribution network load nodes have similar power consumption curves, data mining the different node power consumption curves results in node division. This produces node clusters, thereby reducing the complexity of the distribution network load modeling.

C. PHOTOVOLTAIC (PV) CLUSTER OUTPUT STATE MODELING

1) PROBABILITY DENSITY MODEL FOR THE LIGHT INTENSITY

Typically, a PV output is approximately linearly correlated with the light intensity. The light variation obeys a Beta distribution. A probability density function of the light intensity can be established based on (5) [33] as follows:

$$f_s(x_s) = \frac{\Gamma(\alpha_{Ir} + \beta_{Ir})}{\Gamma(\alpha_{Ir})\Gamma(\beta_{Ir})} (x_s)^{\alpha_{Ir}-1}(1 - x_s)^{\beta_{Ir}-1}, \tag{5}$$

where $\Gamma(\cdot)$ is the gamma function. In addition, $x_s = S_{Ir,t}/S_{Irref,t}$. $S_{Ir,t}$ is the light intensity at a time t. $S_{Irref,t}$ is the baseline light intensity on a clear day at the time t; it can be taken as a fixed baseline light or can be dynamically corrected according to different regions and seasons. In this study, the average baseline light for each season is calculated under local cloud-free conditions; however, when the historical light data at a certain time is larger than that of the baseline light, it is calculated according to the baseline light data. Moreover, α_{Ir} and β_{Ir} are the Beta distribution shape parameters. These can be approximated using the mean value μ_{Ir} and standard deviation σ_{Ir} of the ratio of the light intensity historical data to the baseline light data, where $\alpha_{Ir} = \mu_{Ir}[\mu_{Ir}(1 - \mu_{Ir})/\sigma_{Ir}^2 - 1]$, and $\beta_{Ir} = \alpha_{Ir}(1 - \mu_{Ir})/\mu_{Ir}$.

According to the probabilistic light intensity model established based on (5), the cloud state affects the model parameters; thus, the state needs to be divided.

2) CLOUD STATE DIVISION

The cloud coverage level (CCL) indicator indicates the change in the cloud cover status. The cloud coverage level at a certain time of day t is established using (6) [28].

$$f_{CCL}(t) = 1 - \frac{S_{Ir,t}}{S_{Irref,t}} \tag{6}$$

Based on the CCL index, the cloud conditions in a day are divided into L_{Ir} levels. Therefore, the cloud states are divided into several categories. Subsequently, the data for different cloud states are counted according to (6). The probability density parameters for the PV output under different cloud states are calculated according to (5). These can be combined with the baseline light data on a clear day to derive the PV output at different moments using (7) [28] as follows:

$$P_{PV,sim}(t) = Beta(\alpha_{L_{Ir}}, \beta_{L_{Ir}}) \cdot \frac{S_{Irref,t} P_{PV,N}}{S_{Irref}}, \tag{7}$$

where $Beta(\cdot)$ is the Beta distribution function. $\alpha_{L_{Ir}}$ and $\beta_{L_{Ir}}$ are both Beta distribution parameters for the L_{Ir} cloud state. $P_{PV,N}$ is the grid-connected PV power rating. S_{Irref} is the standard light intensity and is taken as 1000 W/m^2 in this study.

D. CONSTRUCTION OF THE SOURCE-LOAD POWER BEHAVIOR STATE TRANSFER MATRIX

Based on the historical data, the probability of the power consumption state shifting at the node load of the distribution network at a time t is calculated using (8) as follows:

$$p_{s_{s,c},s_{s,l}}(t) = \frac{q_{s_{s,c},s_{s,l}}(t)}{\sum_{s_{s,l}=1}^{K} q_{s_{s,c},s_{s,l}}(t)}, \tag{8}$$

where $q_{s_{s,c},s_{s,l}}(t)$ represents a sample of the time slot state $s_{s,c}$. Here, the station is located at the moment t and is transferred to the state $s_{s,l}$ after one step.

By applying (5) and (6) to the light data, the probability of the cloud state shifting at any moment $t\boldsymbol{P}_c(t)$ under a time interval t_{cd} is calculated according to the cloud state using (9).

$$p_{c,s_{cs,c},s_{cs,l}}(t) = \frac{q_{c,s_{cs,c},s_{cs,l}}(t)}{\sum_{s_{s,l}}^{L_{Ir}} q_{c,s_{cs,c},s_{cs,l}}(t)}. \tag{9}$$

In the above, $q_{c,s_{cs,c},s_{cs,l}}(t)$ is a sample of the cloud state $s_{cs,c}$ at the moment PV t after a one-step transfer to the state $s_{cs,l}$.

When the number of samples is sufficiently large, the numbers of statistical samples in (8) and (9) tend to be probabilistically distributed. The transfer probability can be approximated using a statistical representation of the historical samples. This is used in the construction of the distribution network node power consumption transfer matrix.

Based on the initial state of electricity consumption, state transfer matrix, and power probability density corresponding to each state, the power curves of the distribution network node load and PV for one day can be obtained for the construction of the distribution network uncertain operation scenario. In the power dispatch interval, the load power curve is treated linearly, whereas the PV power output is solved according to a data-driven solution. Specifically, the PV power output state transfer probability of two adjacent power dispatch moments is used as the PV power output state transfer probability in the power dispatch interval. Additionally, the PV power output state during the regulation command interval can be determined according to (2) and (3). The PV power output value is obtained by combining the power probability densities of this state.

III. NETWORK CONTROL OF THE DISTRIBUTED PV CLUSTER CONFIGURATION

Typically, inverters can use the residual capacity for reactive power compensation. They can be classified according to the type of reactive power compensation into GFL and GFM inverters [34]. The external characteristics of GFL inverters are expressed as current sources and those of the GFM inverters are expressed as voltage sources. Owing to the frequent light fluctuations and substantial uncertainty, a PV inverter's DC voltage is unstable; thus, GFL control is typically used. However, it is difficult to ensure standard PV generation when GFM control is used. The remaining PV capacity randomly fluctuates, making it challenging to maintain the voltage stability of the grid. This section proposes a control structure for ensuring the average grid-connected power generation of the distributed PVs while actively supporting reactive voltage regulation.

A. ANALYSIS OF THE REACTIVE POWER COMPENSATION MECHANISM OF INVERTER FOLLOWING-/CONFIGURATION NETWORK-TYPE CONTROL

Most GFL inverters use the component forms of the d-axis and q-axis to independently control the active and reactive power, as shown in (10) as follows:

$$\begin{cases} p = u_q i_q \\ q = u_q i_d \end{cases} \tag{10}$$

where p and q are the instantaneous active and reactive powers of the inverter, respectively. u_q is the instantaneous value of the d-axis voltage component of the bus voltage after the Pike transformation. i_d and i_q are the instantaneous values of the d-axis and the q-axis current components of the inverter after the Pike transformation of the three-phase current, respectively.

The GFM inverter simulates the characteristics of a synchronous generator to regulate the grid operation. Taking the sag control as an example, the voltage angular velocity of the inverter control output ω_0 and voltage amplitude U_0 control can be expressed using (11) as follows:

$$\begin{cases} \omega_0 = \omega_{ref} + k_r(P_{ref} - P) \\ U_0 = U_{ref} + k_q(Q_{ref} - Q) \end{cases} \tag{11}$$

where ω_{ref} and U_{ref} are the grid frequency and voltage amplitude of the inverter control reference, respectively. P_{ref} and Q_{ref} are the active and reactive power of the inverter control reference, respectively. P and Q are the actual output active power and reactive power of the inverter, respectively. k_r is the sag factor for controlling the active power by adjusting the grid frequency; k_q is the sag factor for controlling the reactive power by adjusting the grid voltage.

The GFM inverter produces active and reactive power to regulate the bus voltage amplitude and its phase angle to obtain the desired results. Owing to the unstable PV power output, the active power output cannot be adjusted following a grid voltage change. Additionally, its residual capacity is uncertain and the reactive power output is unstable. The use of conventional inverters with GFM control makes it difficult to achieve the effect of frequency and voltage regulation. Thus, an energy storage device is typically added to the DC side to control the active power output, but this increases the investment costs. According to (10)–(11), the reactive power alone can also be used to simulate the GFM network characteristics. Thus, this study focuses on the relationship between the reactive power and voltage; the GFM network characteristics of the active power and frequency are ignored when considering the role of the GFM-network-type inverter.

B. COORDINATED CONTROL OF MULTIPLE PV ARRAYS

A conventional DPV generation system consists of a PV string and grid-tied inverter. In the PV string, several PV panels are connected in series and several strings of PV panels are connected in parallel to one inverter. Typically, several

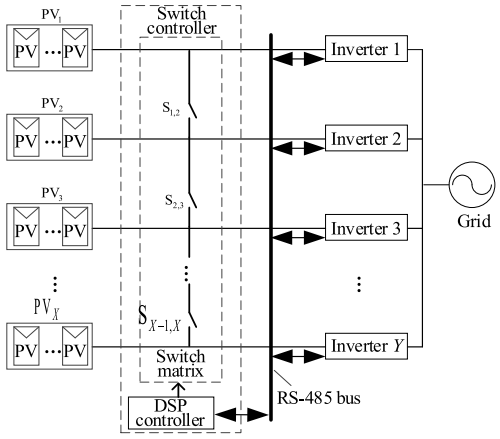

FIGURE 2. Distributed photovoltaic (DPV) cluster control system topology.

inverters are connected in parallel to the grid for regular operation [35].

The PV group control system comprises PV strings, inverters, and a reconfigurator. The *X* group of the PV strings and *Y* group of the grid-tied inverters are flexibly connected through the reconfigurator, as shown in the topology of the PV group control system in Fig. 2. The reconfigurator is placed on the inverter side to connect the PV strings and inverters and the PV string and grid-tied inverter are connected to the reconfigurator through the DC cable plug. The reconfigurator and inverter are also connected to a communication interface to transmit data [35]. The inverter contains current and voltage sensors for data calculations based on electrical measurement information regarding the connection between the inverter and PV array, thereby reducing the investment cost. Owing to its reduced communication configuration and calculation requirements, the inverter *Y* can be efficiently employed for the control of the group control system operations, further reducing the investment cost.

All connections between the PV strings and inverters and starts/stops of the inverters are controlled. In low-irradiance conditions, the parallel-bridge switches to control the *N* group of PV strings, which are connected in parallel to one of the inverters for generating GFL control power. The other inverters are free to switch to GFM or GFL control according to the scheduling commands. When the irradiance is sufficiently strong, the connection is returned to the normal mode and the inverters are all controlled in the GFL mode. Similarly, the irradiance (from strongest to weakest process) and number of inverters connected to the PV strings connected across the bridge-switch gradually changes from *Y* to one. The inverters in the free state will be disconnected from the PV strings and will only provide reactive power to the grid. They can be freely switched to GFM or GFL control as needed.

IV. DISTRIBUTION NETWORK CONFIGURATION/FOLLOWING NETWORK EQUIPMENT COLLABORATIVE OPTIMAL CONFIGURATION

To reduce the overlaps in the reactive power resource management areas, the reactive power management areas in the distribution networks are divided according to the reactive power zoning method mentioned in [19]. In addition, the dedicated reactive power equipment are placed according to the sensitivity of different zoning nodes. Based on the fast- and slow-response characteristics of the GFM and GFL reactive power equipment, a multi-timescale collaborative optimal allocation strategy is proposed for reactive power resources. The optimal configuration model is established with the primary decision objective of minimizing the configuration cost of the dedicated reactive power equipment and auxiliary decision objective of minimizing the voltage deviation of the entire network throughout the day. The primary decision provides the configuration scheme for the auxiliary decision; the auxiliary decision provides the desired configuration capacity for the dedicated reactive equipment. Finally, the configuration results for the dedicated reactive equipment are obtained according to continuous iterative corrections. In this study, a shunt capacitor bank (SCB) and SVG are used as examples of the dedicated equipment.

A. SITE SELECTION FOR DEDICATED REACTIVE POWER EQUIPMENT

In this study, a zoned reactive power compensation method is used to divide the distribution network area. The desired installation locations for the reactive power equipment within the zoned areas are selected according to a node voltage/reactive power sensitivity index [19]. Based on the reactive power zoning method in [19], the node sensitivity index is used to divide the reactive power regions. The nodes corresponding to the maximum average sensitivity degree in the different areas are then taken as the dominant nodes in the region.

The partitioning results of the distribution network change as the grid operation scenarios change. The dominant nodes in all of the regions of each scenario correspond to one configuration scheme. When studying the optimal cooperative allocation strategy for distributed reactive power resources, the dominant nodes selected from regions in different operation scenarios should be comprehensively considered. Considering each partition result, the dominant node numbers are arranged in descending order. The proportion of dominant nodes in each region is counted and the node numbers below a certain probability value are discarded. The remaining node numbers are selected as the set of dominant nodes. They are used as the candidate installation locations for the SCB and SVG to ensure the optimization of the regionalized reactive power of the distribution network and improve the adaptability of the strategy.

B. CONSTRUCTION OF OPTIMAL REACTIVE POWER ALLOCATION MODEL CONSIDERING PRIMARY/AUXILIARY DECISIONS

Owing to the load and PV fluctuations, it is difficult to maintain a minimum voltage deviation for the entire network for a long time when only considering the time of the command issuance. Therefore, it is necessary to also consider the volt-

age distribution of the distribution network during the interval between two commands to minimize the voltage deviation in the entire network during that time. Then, the reactive power output during the interval between two power dispatch commands can be changed using the SVG or PV inverter configuration network-type control and autonomously regulated voltage.

1) OBJECTIVE FUNCTION

a: ASSISTED DECISION-MAKING OBJECTIVES

The distribution network load and PV one-day operations vary as an all-day operation scenario. The sum of the voltage deviations in the entire network in the all-day operation scenario is minimized as the auxiliary decision objective to establish the objective function F_2. This is shown in (12) as follows:

$$\min F_2 = \sum_{t=1}^{T_m} \sum_{i=1}^{n} \left| U_{t,i} - U_0 \right|, \tag{12}$$

where T_m is the total number of moments in a day, and n is the number of system nodes. $U_{t,i}$ is the voltage of node i at moment t; U_0 is the nominal value of the node voltage.

To maximize the PV inverter's configuration network control function and reduce the dedicated reactive equipment configuration capacity, it is necessary to ensure that the DPV group control system generates power while maximizing the number of free states of the inverters. The operation target used to establish the DPV group control system is shown in (13) as follows:

$$\max F_3 = f_{t,i}(P_{\mathrm{PVinv}}) \cdot n_{\mathrm{fr},t,i}, \tag{13}$$

where $f_{t,i}(P_{\mathrm{PVinv}})$ is the output power of the DPV cluster control system at node i during time t. $n_{\mathrm{fr},t,i}$ is the number of free-state inverters in the DPV cluster control system at node i during time t.

The solution of (13) can be determined according to the switching connection states of the DPV group control system, where the number of selectable switching connection states is small. Thus, an exhaustive method can be used to obtain the number of free-state inverters and total output power of the group control system under different switching connection methods.

b: PRIMARY DECISION OBJECTIVES

When configuring SCBs and SVGs for different reactive power partitions, the auxiliary decision optimizes the set of uncertain operation scenarios to derive the desired capacity for the reactive power equipment under different scenarios. By contrast, the primary decision optimizes the final configuration scheme based on the desired capacity. The objective function for the total investment cost of reactive equipment is established using (13) [25] as follows:

$$\min C = C_{\mathrm{fi}} + C_{\mathrm{om}}, \tag{14}$$

where C is the total investment cost, and C_{fi} and C_{om} are the annual investment cost and operations and maintenance (O& M) costs of the reactive equipment, respectively.

The annual investment cost is calculated using (14) based on the equal annual output value method C_{fi}. Put another way, it is based on the fixed investment costs of the SCB, SVG, and PV cluster control systems. The calculations are shown in (15) [25] as follows:

$$\begin{cases} C_{\mathrm{fi}} = C_{\mathrm{SCBfi}} + C_{\mathrm{SVGfi}} + C_{\mathrm{PVfi}} \\ C_{\mathrm{SCBfi}} = R_{\mathrm{SCBfi}} \sum_{i=1}^{n} (S_{\mathrm{SCB},i} c_{\mathrm{SCB}}) \\ C_{\mathrm{SVGfi}} = R_{\mathrm{SVGfi}} \sum_{i=1}^{n} (S_{\mathrm{SVG},i} c_{\mathrm{SVG}}) \\ C_{\mathrm{PVfi}} = R_{\mathrm{PVfi}} \sum_{i=1}^{n} (S_{\mathrm{PVfi},i} c_{\mathrm{PVfi}}) \\ R = \frac{r(1+r)^{L_f}}{(1+r)^{L_f}-1} \\ S_{\mathrm{SVG},i} = n_{\mathrm{INSSVG},i} Q_{\mathrm{SVGmax},i} \\ S_{\mathrm{SVG},i} = n_{\mathrm{INSSCB},i} Q_{\mathrm{SCBmax},i} \end{cases} \tag{15}$$

where C_{SCBfi}, C_{SVGfi}, and C_{PVfi} are the annual investment costs of the SCB, SVG, and PV group control systems, respectively. $S_{\mathrm{SCB},i}$, $S_{\mathrm{SVG},i}$, and $S_{\mathrm{PVfi},i}$ are the SCB configuration capacity, SVG configuration capacity, and total PV group control system capacity at node i, respectively. $Q_{\mathrm{SVGmax},i}$ and $Q_{\mathrm{SCBmax},i}$ are the minimum capacity of the SVG single unit and SCB capacity per group at node i, respectively. $n_{\mathrm{INSSVG},i}$ is the number of SVG single units installed at node i; $n_{\mathrm{INSSCB},i}$ is the number of SCBs per group installed at node i. c_{SCB}, c_{SVG}, and c_{PVfi} are the unit capacity costs of the SCB, SVG, and PV group control systems, respectively. R_{SCBfi}, R_{SVGfi}, and R_{PVfi} are the equal annual value coefficients of the SCB, SVG, and DPV group control systems, respectively. r is the depreciation rate of the installed equipment, and L_f is the service life of the installed equipment.

The O&M costs of the SCBs and SVGs (based on a percentage of the fixed investment cost) are calculated using (16) [25] as follows:

$$\begin{aligned} C_{\mathrm{om}} &= C_{\mathrm{SCBom}} + C_{\mathrm{SVGom}} + C_{\mathrm{PVom}} \\ &= \gamma_{\mathrm{SCB}} C_{\mathrm{SCBfi}} + \gamma_{\mathrm{SVG}} C_{\mathrm{SVGfi}} + \gamma_{\mathrm{PV}} C_{\mathrm{PVfi}}, \end{aligned} \tag{16}$$

where γ_{SCB}, γ_{SVG}, and γ_{PV} are the ratios of the O& M costs of the SCB, SVG, and PV group control systems to the investment, respectively.

2) CONSTRAINTS

The system constraints are required to satisfy the equation and inequality constraints, including the data sampling moment and sampling interval time period. Taking the moment t as an example, the equation and inequality constraints are established based on (17)–(21).

Both the SCB and SVG optimal joint configuration models should satisfy the system power balance constraint shown

in (17) as follows:

$$\begin{cases} P_{t,i} = U_{t,i} \sum_{j=1}^{n} U_{t,j}(G_{ij}\cos\theta_{t,ij} + B_{ij}\sin\theta_{t,ij}) \\ Q_{t,i} = U_{t,i} \sum_{j=1}^{n} U_{t,j}(G_{ij}\sin\theta_{t,ij} - B_{ij}\cos\theta_{t,ij}) \\ P_{t,i} = P_{\mathrm{L},t,i} - P_{\mathrm{PV},t,i} \\ Q_{t,i} = Q_{\mathrm{L},t,i} - Q_{\mathrm{PV},t,i} - Q_{\mathrm{SCB},t,i} - Q_{\mathrm{SVG},t,i} \end{cases} \tag{17}$$

where $P_{t,i}$ and $Q_{t,i}$ are the active and reactive power injected into node i at a time t, respectively. $\sum_{i=1}^{n} P_{t,i} > 0$. $P_{\mathrm{PV},t,i}$ and $Q_{\mathrm{PV},t,i}$ are the active and reactive power outputs from the DPV inverter at node i during time t, respectively. $P_{\mathrm{L},t,i}$ and $Q_{\mathrm{L},t,i}$ are the active and reactive power consumed by the load at node i during time t, respectively. $Q_{\mathrm{PV},t,i}$, $Q_{\mathrm{SCB},t,i}$, and $Q_{\mathrm{SVG},t,i}$ are the reactive power compensation capacities of the DPV inverter, SCB, and SVG at node i during time t, respectively. $U_{t,i}$ and $U_{t,j}$ are the voltages at nodes i and j during time t, respectively. B_{ij} and $\theta_{t,ij}$ are the effective values of the voltage at nodes i and j during time t, respectively. G_{ij} is the line conductance and electroneutrality between node i and node j; $\theta_{t,ij}$ is the voltage phase angle difference between node i and node j at time t.

Considering the slow response of the SCB reactive power compensation tracking and limitation on the number of cuttings in a day, the SCB cuttings also need to meet the minimum time of 1 h. The SCB reactive power compensation constraint is calculated as follows:

$$\begin{cases} 0 \le N_{\mathrm{C},t,i} \le N_{\mathrm{C\,max}} \\ Q_{\mathrm{SCB},t,i} = N_{\mathrm{C},t,i} \cdot q_{\mathrm{C}} \\ \sum_{t=1}^{T_{\mathrm{m}}} k_{\mathrm{C},t,i} \le K_{\mathrm{C}} \end{cases} \tag{18}$$

where $N_{\mathrm{C},t,i}$ is the number of SCB cut groups at node i during moment t; $N_{\mathrm{C\,max}}$ is the maximum number of SCB groups; q_C is the SCB single group cut capacity; $k_{\mathrm{C},t,i}$ is the number of capacitors switching at node i during moment t in the distribution network, where $k_{\mathrm{C},t,i} \in \{0, 1\}$; and K_{C} is the maximum allowable number of SCB switching groups.

Assuming that the same capacity of the single inverter is used at the same node, the PV inverter reactive power compensation constraint is as follows:

$$\begin{cases} Q_{\mathrm{PVm}ax,t,i} = \sqrt{S_{\mathrm{ins},i}^2 - P_{\mathrm{PV},t,i}^2} \\ Q_{\mathrm{PV},t,i} = Q_{\mathrm{PVGFM},t,i} + Q_{\mathrm{PVGFL},t,i} \\ Q_{\mathrm{SVG},t,i} = Q_{\mathrm{SVGGFM},t,i} + Q_{\mathrm{SVGGFL},t,i} \\ -Q_{\mathrm{PVm}ax,t,i} \le Q_{\mathrm{PV},t,i} \le Q_{\mathrm{PVm}ax,t,i} \\ -n_{\mathrm{fr},t,\mathrm{i}} S_{\mathrm{inv},i} \le Q_{\mathrm{PVGFM},t,i} \le n_{\mathrm{fr},t,\mathrm{i}} S_{\mathrm{inv},i} \\ -S_{\mathrm{SVG},i} \le Q_{\mathrm{SVG},t,i} \le S_{\mathrm{SVG},i} \\ Q_{\mathrm{SCB},t,i} \le S_{\mathrm{SCB},i} \\ n_{\mathrm{GFM},t,i} \le n_{\mathrm{frmax},t,i} \\ Q_{\mathrm{GFM},t,i} \le n_{\mathrm{GFM},t,i} S_{\mathrm{inv},i} \end{cases} \tag{19}$$

where $Q_{\mathrm{PVm}ax,t,i}$ is the remaining PV inverter capacity at node i during time t; $S_{\mathrm{ins},i}$ is the installed PV capacity at node i; and $S_{\mathrm{inv},i}$ is the capacity of the single inverter at node i. $Q_{\mathrm{PVGFM},t,i}$ and $Q_{\mathrm{PVGFL},t,i}$ are the reactive power outputs of PV inverters with GFL and GFM control at node i during time t, respectively. $Q_{\mathrm{SVGGFM},t,i}$ and $Q_{\mathrm{SVGGFL},t,i}$ are the reactive power outputs of SVGs with GFL and GFM control at node i during time t, respectively. $n_{\mathrm{GFM},t,i}$ and $n_{\mathrm{frmax},t,i}$ are the number of inverters with GFM control and maximum number of inverters in the system in the free state at node i during time t, respectively.

Ignoring the difference between the rated power and maximum input power of the PV inverters, the DPV cluster control system must satisfy (20) at every switching as follows:

$$P_{\mathrm{inv,input}} \le S_{\mathrm{inv,N}}, \tag{20}$$

where $P_{\mathrm{inv,input}}$ and $S_{\mathrm{inv,N}}$ are the input power and rated power of any inverter, respectively, and $S_{\mathrm{inv,N}} \le S_{\mathrm{inv},i}$.

Chance-constrained planning is used to obtain the description of the distribution network pollution uncertainty in the form of a probability. This allows the node voltage to cross the limit at a certain confidence level. The node voltage chance constraint is established as follows:

$$P_{\mathrm{r}}\{U_{\mathrm{N\,min}} \le U_{t,i} \le U_{\mathrm{N\,max}}\} > \alpha_{\mathrm{con}}, \tag{21}$$

where $U_{\mathrm{N\,max}}$ and $U_{\mathrm{N\,min}}$ are the upper and lower voltage limits of the nodes, respectively. α_{con} is the confidence level that the voltage will not cross the limit at time t.

C. DISTRIBUTION NETWORK AND RESOURCES COOPERATIVE ALLOCATION STRATEGY

As described below, the reactive equipment capacity of each partition is randomly provided based on the primary decision. The configuration scheme is passed to the auxiliary decision optimization, which optimizes the desired configuration capacity for the optimal operation of the reactive equipment and passes it to the primary decision optimization. The primary decision selects the equipment configuration scheme according to the desired configuration capacity. It then calculates the configuration investment cost before passing the configuration scheme to the auxiliary decision to ensure optimal operation. Finally, the final configuration optimization result is obtained by continuously correcting the primary decision configuration scheme. In this study, the solution results for the decision objective are the reactive power compensation capacities for each equipment in the reactive power partitions meeting the minimum voltage deviation for the operation scenario. This includes the desired operating capacities of the SCBs and SVGs in the dominant node of each reactive power partition. Here, the solution result of the primary decision objective is the minimum investment cost of each reactive power equipment, including the installed capacities of the SCB and SVG equipment.

1) COOPERATIVE/CONTROL RELATIONSHIP BETWEEN REACTIVE EQUIPMENT

This study uses SCB, SVG, and PV inverters to represent traditional, dedicated, and compatible equipment, respectively.

TABLE 1. Control command update level division of reactive power equipment.

Reactive equipment	Control type	Control instruction response cycle	Engageable reactive optimization layer
Shunt capacitor bank (SCB)	Grid-following (GFL) control	Hour cycle	Level 1
Static var generator (SVG), photovoltaic (PV) inverters	GFL control	Power-dispatching instruction cycle	1st and 2nd levels
SVG, PV inverters	Grid-forming (GFM) control	Real-time	1st, 2nd, and 3rd levels

These equipment are analyzed and graded from the perspective of the equipment tracking response capability to provide constraints for the subsequent optimal allocation of the voltage reactive power in the distribution networks. Based on the analysis of the dedicated and part-time reactive power equipment and reactive power command control type, the speeds of the SCB, SVG, and PV inverters are classified from the perspective of the time of issuance of the power dispatch command, as shown in Table 1. The SVG and PV inverters have similar characteristics, and their GFL control mainly follows the power-dispatching command. Additionally, their GFM control has a faster response time (corresponding to the first and second reactive power optimization layers of the distribution network). Moreover, the reactive power output can be freely controlled during the intervals between power-dispatching commands. The reactive power commands are equivalent to real-time adjustments. The adjustable cycle response of the GFM control is the fastest, and corresponds to the third layer of the distribution network reactive power optimization. The grid capacity can also be used for optimization in the first two layers if the reactive power optimization is insufficient. Using multiple hourly reactive equipment, command cycles with power dispatching, and real-time scaling, a multi-time scale [36] cooperative control relationship can be used to provide the basis for the subsequent establishment and solution of the reactive power optimization configuration model.

2) REACTIVE EQUIPMENT CO-CONFIGURATION STRATEGY AND SOLUTION

The configuration of the equipment should prioritize low-cost equipment while considering the variability in the cost and performance of each reactive equipment to meet both the primary and auxiliary decision objectives. Slow-response equipment should be prioritized during the optimization of the reactive power in the envisioned operation scenario. This study uses a linearly decreasing weight particle swarm optimization (LinWPSO) algorithm [37] to solve for the optimal configuration model using the following steps. Step 1: According to each reactive power partition, the initial value of the primary decision is provided, i.e., the configured capacity of the SCB and SVG in each partition is randomly provided. The scheme is then passed to the auxiliary decision. Step 2: The amount of optimization at each level is calculated based on the multi-time scale reactive power optimization. Based on the reactive power equipment responsiveness, it is known that the SCB hourly level regulation should be prioritized for the reactive power optimization. The LinWPSO algorithm is used to calculate the optimal amount of reactive power operation for this time scale. This optimal amount is then used to obtain the reactive power operation curves of the dedicated and part-time reactive equipment at the hourly level of each partition. Subsequently, the curves are used as the first layer of reactive power regulation curves. If the PV installation and dominant nodes of the partition are in the same location, the reactive power control quantities of the dedicated and part-time equipment after superposition are equal to the total amount. The priority of the reactive power optimization for the part-time equipment is higher to reduce the investment cost of dedicated equipment. By contrast, if the locations of the two equipment are different, the reactive power control curves of the dedicated and part-time equipment are optimized separately and the same principle is used for each layer of the reactive power optimization curve. Step 3: Considering the limitation on the number of times that SCB switching can occur in a day, the number of SCB switching groups and reactive power output of the gird-following control equipment are used as the control variables to optimize the calculations at each moment. Additionally, the optimal partitioning method is used to divide the optimization results for the first layer of dedicated reactive power equipment. The action moment of each SCB partition and its switching capacity is obtained. Finally, the desired configuration capacity of the SCB and first layer of the reactive power optimization are obtained. Step 4: Considering the medium-speed response capability of the equipment, the time scale scenario of the dispatch command cycle is optimized for the reactive power of the following network type (which is based on the reactive power regulation volume of the first layer). The reactive power operation curves for each partition's dedicated and part-time following network-type equipment are then obtained. Step 5: Considering the fast-response capability of the equipment, the GFM reactive power equipment is selected to optimize the reactive power for the operation scenarios with time stamps in their distribution network based on the second layer of the reactive power regulation volume. The reactive power operation curve of the dedicated and auxiliary GFM equipment in each partition is then obtained and used as the third layer of the reactive power regulation curve. Step 6: The SVG is superimposed with the GFL control reactive operation curves at the first and second layers to obtain the desired configuration capacity of the GFL SVG. Step 7: Based on the reactive power regulation curve of the third layer, the desired configuration capacity of the GFL SVG is determined. Finally, desired configuration capacity of the SVG

TABLE 2. PV inverter allocation information in IEEE 33-Node system.

Access location	5	8	17	24	28	32
Number of PV inverters	16	16	16	8	8	16

is determined by combining the configuration information from the GFL SVG obtained in Step 6. Step 8: The frequency probability is used to estimate where the voltage-crossing chance constraint holds. The desired configuration capacity of the dedicated reactive equipment with a confidence level is passed to the primary decision optimization to modify the configuration scheme, which is then passed to the auxiliary decision optimization. Step 9: Steps 2 to 8 are repeated until the confidence convergence condition is reached, resulting in the optimal reactive power equipment configuration scheme. In solving the problem of the reactive power device capacity allocation in this study, the main computational time is occupied by the optimization calculations for the primary and auxiliary decision processes. We employ the notation $\boldsymbol{O}$ () to analyze the time complexity of the entire process. We initially estimate the worst-case time complexity of the proposed method as $\boldsymbol{O}$ ($B_{\mathrm{TC}} \times (M_{\mathrm{TC1}} \times N_{\mathrm{TC1}} + M_{\mathrm{TC1}} \times M_{\mathrm{TC2}} \times N_{\mathrm{TC2}} \times I_{\mathrm{TC}}) + C_{\mathrm{TC}}$). In this estimation, B_{TC} represents the number of time windows. M_{TC1} represents the number of particles in the upper-level model, N_{TC1} represents the number of iterations in the upper-level model, and M_{TC2} represents the number of particles in the lower-level model of the particle swarm algorithm. N_{TC2} represents the number of iterations in the lower-level model of the particle swarm algorithm, I_{TC} represents the number of times the power flow calculation is performed in the lower-level model. C_{TC} represents the constant time complexities.

V. CASE STUDY ON IEEE 33-NODE SYSTEM

To verify the effectiveness of the proposed strategy, the IEEE 33-node system is used as a case study for the configuration of dedicated reactive equipment. The uncertain operation scenario of the distribution network is constructed using the source-load modeling method described in Section I. In addition, 500 scenarios are extracted for simulation using the Monte Carlo method based on modeling parameters obtained from the literature [28]. The optimal access locations and capacities of the SCB and SVG are investigated when the PV configuration information is known. The distribution network line parameters are referenced from [38], where the main transformer capacity is 6 MVA. Table 2 shows the known PV configuration information, where four PV inverters are selected to form a cluster control system for nodes 5, 17, 24, and 28. Considering that the highest cost item in the PV cluster control system is the control switch, the unit capacity costs of the PV cluster control system c_{PVfi} is set to \$ 8/kW. The service lives of the SCB, SVG, and PV cluster control systems L_{f} are 10 years, 15 years, and 20 years, respectively. The other parameters are shown in Table 3.

TABLE 3. Parameters used in IEEE 33-Node system.

Symbol	Parameter Variables	Specification
$Q_{\mathrm{SCBmax},i}$	SCB capacity per group at node i	100 kvar
c_{SCB}	SCB installed cost per unit capacity	50 RMB/kvar[39]
K_{C}	SCB Threshold for the number of cuttings in a day	five times
$Q_{\mathrm{SVGmax},i}$	minimum capacity of SVG single unit at node i	50 kvar
c_{SVG}	SVG installation cost per unit capacity	200 RMB/kvar[39]
$S_{\mathrm{inv,N}}$	rated output power of single PV inverters	36 kW
$S_{\mathrm{inv},i}$	maximum apparent power of single PV inverters at node i	40 kVA
r	Equipment depreciation rate	6%
γ_{SCB} , γ_{SVG} and γ_{PV}	Equipment operation and maintenance (O&M) cost factors	5%
$U_{\mathrm{N\,max}}$ and $U_{\mathrm{N\,min}}$	the upper and lower voltage limits of the nodes	±5%
α_{con}	Degree of confidence	0.95

A. APPLICATION OF MARKOV CHAIN FOR TRANSITION OF BEHAVIOR STATE

This section analyzes the application of Markov chains and sequential Monte Carlo sampling for the duration of the behavior states. By utilizing historical data on the local distribution grid loads and solar irradiance, the random behavior states of the source-load interaction are partitioned into intervals. Then, a stochastic Markov model is established to capture their probabilistic behaviors. Based on the Markov models of the load and PV random behaviors in each time period, the future scenarios are subjected to a sampling analysis. The more granular the classification of load and PV output behavior states, the higher the computational accuracy; however, this also entails an increase in computational complexity. Typically, it is recommended to classify the states into three to five categories for a suitable level of accuracy. Here, we illustrate the case by dividing the behavior states of the PV output and load into four categories.

Considering the operating scenarios of the PV output as an example, the different cloud layer states and corresponding irradiance data are obtained using (6). The PV outputs under different cloud layer states are obtained using (7). The CCL index is divided into four levels: L_{Ir1}, L_{Ir2}, L_{Ir3} and L_{Ir4}, as shown in Table 4. The smaller the CCL value, the less the cloud cover and better the irradiance.

Owing to the correlations between the behavior states of the PV output and CCLs, the Markov chain is employed to obtain the interrelationships between the PV output behavior states at different time points. This results in a probability transition matrix. This study considers a time period from 9 AM to 12 PM, totaling 180 min, as an example for the case study. The initial probability of the PV behavior states is defined based on (22), where each column of (22)

TABLE 4. Cloud coverage level (CCL) classification.

CCL	CCL indicator range	Beta distribution shape parameters	
		α_{Ir}	β_{Ir}
L_{Ir1}	0.00–0.25	12.97	1.86
L_{Ir2}	0.25–0.55	19.06	12.37
L_{Ir3}	0.55–0.85	8.34	18.78
L_{Ir4}	0.85–1.00	2.23	29.05

represents the initial probabilities for the four behavior states of the PV output. The transition probability matrices between the different states are represented by (23) to (25).

$$\boldsymbol{P}_{\mathrm{pv0}} = [0.4763\ 0.3773\ 0.0474\ 0.0991] \tag{22}$$

$$\boldsymbol{P}_{\mathrm{pv,9\_10}} = \begin{bmatrix} 0.6042 & 0.3055 & 0.0903 & 0.0000 \\ 0.0499 & 0.8252 & 0.1235 & 0.0014 \\ 0.0482 & 0.1930 & 0.7281 & 0.0307 \\ 0.0000 & 0.0526 & 0.2106 & 0.7368 \end{bmatrix} \tag{23}$$

$$\boldsymbol{P}_{\mathrm{pv,10\_11}} = \begin{bmatrix} 0.5726 & 0.3479 & 0.0795 & 0.0000 \\ 0.0744 & 0.8544 & 0.0712 & 0.0000 \\ 0.2000 & 0.3000 & 0.4857 & 0.0143 \\ 0.0000 & 0.0000 & 0.1333 & 0.8667 \end{bmatrix} \tag{24}$$

$$\boldsymbol{P}_{\mathrm{pv,11\_12}} = \begin{bmatrix} 0.7596 & 0.2019 & 0.0385 & 0.0000 \\ 0.1873 & 0.6889 & 0.1238 & 0.0000 \\ 0.2500 & 0.2292 & 0.5000 & 0.0208 \\ 0.0000 & 0.0000 & 0.0769 & 0.9231 \end{bmatrix} \tag{25}$$

The operational scenarios for the PV output behavior states can be generated based on (22) to (25). Simultaneously, the PV output curve can be obtained by considering the PV output behavior state categories at each time point, Beta distribution shape parameters, and (7). An operational scenario for the PV output curve and PV output behavior states is shown in Fig. 4. It can be observed that within the 0–90 min period, the PV system starts in state category 1 at time 0, remains in this state for 15 min before transitioning to state category 4. Then, after another 15 min, it transitions to state category 2. It subsequently undergoes a self-transition to maintain state category 2 until approximately 90 min, at which point it transitions back to state category 1. By following this transition pattern, the PV output behavior states continue until the 180-min mark, when the PV system ends up in state category 4.

Similarly, the load information can be statistically analyzed to generate Markov state transition probability matrices for the five typical load categories during different time periods. This facilitates an understanding of the relationships between different load states and the generation of load behavior state transition scenarios. This approach follows the same principles as the PV behavior state modeling and will not be further elaborated upon here.

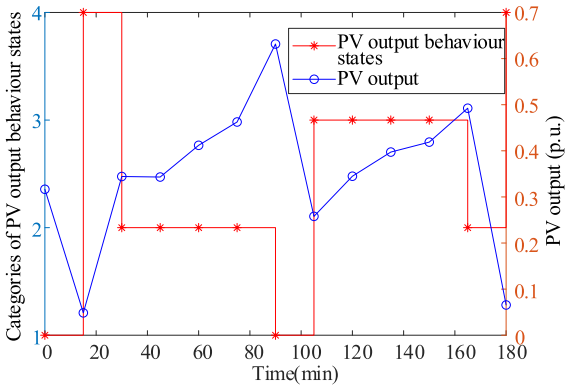

FIGURE 3. Photovoltaic (PV) output and its behavior status curve within 3 h.

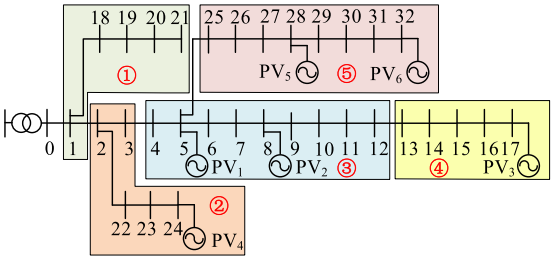

FIGURE 4. Division of the reactive power area in the IEEE 69-node system.

B. ANALYSIS OF DISTRIBUTION NETWORK AREA DIVISION AND DOMINANT NODE SELECTION

The distribution network reactive power area is divided based on the method in [19]. The corresponding distribution network area division results for the operation scenario with five areas are shown in Fig. 4. The distribution network in all areas except for area ① appears to be divided into five regions, and all these regions contain PV locations, with some having two PV access locations. The dominant node in each region is determined based on a combination of the node sensitivity calculation and zoning principles.

The different partitioning situations correspond to different operating scenarios of the distribution network. Moreover, because the inherent properties of the line parameters occupy a certain weight, the calculated partitioning results are similar under most scenarios. Ultimately, five associations are selected as the regional partitioning results. The dominant nodes in each region are selected according to the sensitivity. In addition, the proportion of dominant nodes accounted for by each node number is counted. The node numbers with less than a 5% probability are then discarded and the set of dominant nodes is obtained as {8,11,15,17,21,24,25,32}. The node numbers in this set are used as the candidate installation locations for the SCB and SVG to lay the foundation for subsequent analyses of a cooperative and optimal allocation strategy for reactive power equipment in the distribution network.

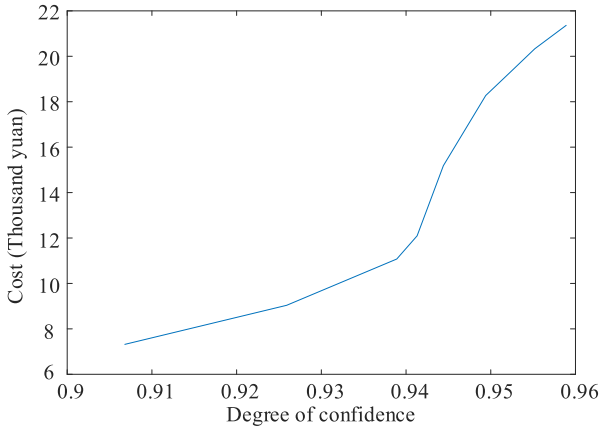

FIGURE 5. Relationship between investment cost and degree of confidence.

TABLE 5. Optimal allocation results for special reactive power equipment.

Scheme	Equipment	Dominant nodes determined	Installed capacity (kvar)	Annual investment cost (thousand yuan)
1	SCB	21, 24	700, 600	20.3
	SVG	8, 17, 21, 32	100, 150, 100, 100	
2	SCB	21, 24	700, 600	25.5
	SVG	8, 17, 21, 32	150, 300, 100, 200	
3	SCB	17, 21, 24, 32	400, 700, 700, 300	49.6
	SVG	8, 17, 21, 24, 32	200, 700, 100, 100, 500	

C. ANALYSIS OF FORMING/FOLLOWING NETWORK REACTIVE POWER RESOURCE COOPERATIVE ALLOCATION STRATEGY

1) COMPARATIVE ANALYSIS OF THE OPTIMIZED CONFIGURATION RESULTS

The reactive power optimization configuration model is solved by selecting dedicated reactive power equipment installation locations based on a set of dominant nodes. In addition, the number of crossing scenarios is counted and the confidence level is calculated until the confidence level requirement is met. The calculations are stopped based on the continuously increasing investment cost and capacity of the equipment configuration at the candidate installation location. Fig. 5 shows the relationship between the investment cost and confidence degree. An increase in the confidence level results in a substantial increase in the investment cost; this increase suddenly accelerates after a certain confidence level is reached. This is mainly owing to the low investment cost required for SCBs compared to SVGs during configuration, which is a priority. The confidence requirement cannot be satisfied after a specific number has been reached; this gradually increases the SVG configuration cost. At this point, increasing the unit confidence requires a more significant investment cost.

The results from the optimal configuration of discrete variables for the dedicated reactive power equipment are shown in Table 5.

All three scenarios are configured by considering both the control mode of the PV inverters and control of the dedicated equipment framing network. Scheme 1 is the strategy proposed in this study, i.e., the PV inverters can follow the network and participate in reactive power optimization. In Scheme 2, the PV inverters can participate in reactive power optimization with grid control [24], [25]. In Scheme 3, the PV inverters do not participate in reactive power optimization [21]. As shown in Table 5, Scheme 1 requires the lowest annual investment cost to satisfy the confidence level requirement. The PV inverter's configuration/following auxiliary network function further reduces the annual investment cost, reflecting the effectiveness of the proposed strategy.

2) ANALYSIS OF EQUIPMENT COLLABORATIVE CONTROL OF HOURLY OPERATION SCENARIOS AFTER CONFIGURATION

Typically, a configuration of dedicated reactive power equipment must reflect the cooperative control of the different equipment in the operation scenario. The proposed control strategy is discussed in this section. Based on the configuration results, a typical operating scenario is selected for the analysis of the cooperative control of different reactive equipment. The total load curve of the typical operational scenario is shown in Fig. 6. Here, the load factor is the ratio of the total load of the distribution network to the transformer capacity. The number of free-state inverters for PV cluster control is analyzed by using the configuration information for the rated capacity of a single inverter as an example. Fig. 7 shows the PV power output standardized value curve for a randomly-selected sunny day scenario, where the quasi-value of the vertical coordinate is based on the rated output power of a single inverter.

The remaining node capacity can be obtained based on its PV output curve and installed PV capacity of the node. The number of free-state PV inverters available at different times is obtained via switching within the PV cluster. The available reactive power capacity for the third level of optimization is obtained using the state inverter. Additionally, because node 24 has an SCB and PV cluster, a three-tier reactive power optimization approach is developed. Taking 17:00–19:00 as an example, the number of free-state inverters in the PV cluster control system of node 24, available reactive capacity variation curve, reactive power optimization variation curve of each layer, and voltage deviation of this node are analyzed for the 18^{th} and 19^{th} periods.

Fig. 8 shows the number of node 24 PV inverters in the free state and power available for the active-reactive power compensation during the 18^{th} and 19^{th} periods. It can be seen that the numbers of PV inverters in the free state at 17:00,

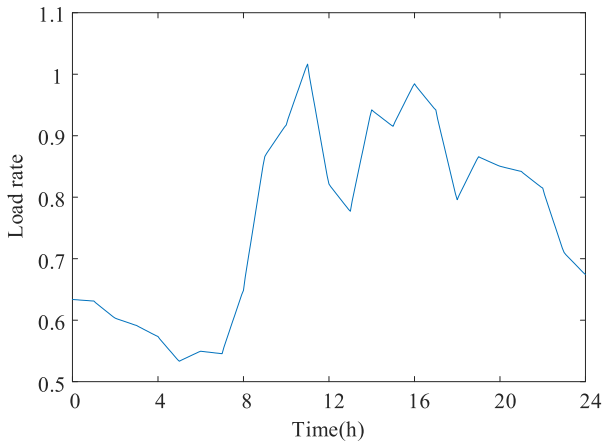

FIGURE 6. Total load curve for a typical operation scenario.

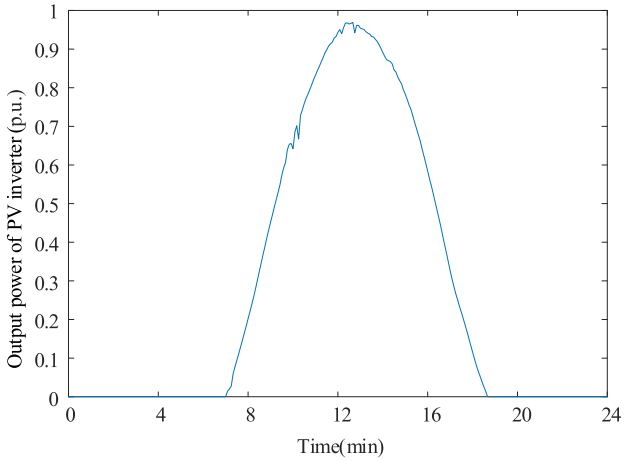

FIGURE 7. PV output curve for a sunny scenario.

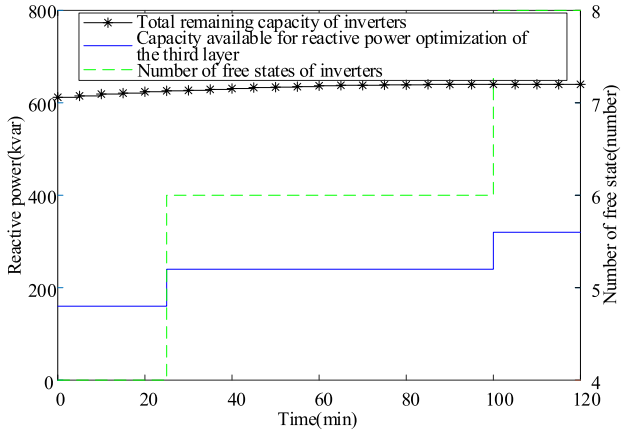

FIGURE 8. Number of free states and residual reactive power of the inverters at node 24.

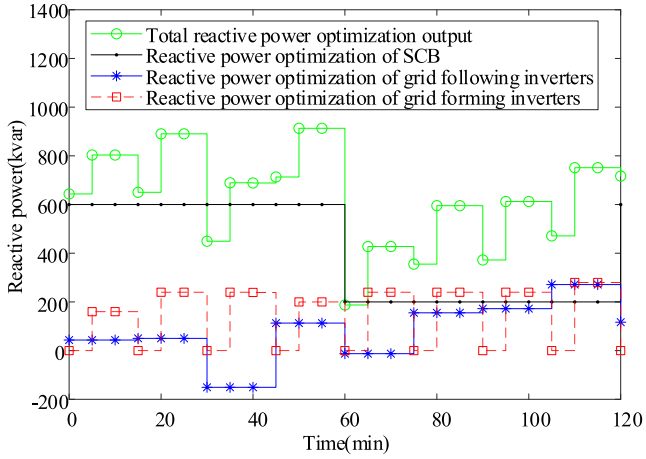

FIGURE 9. Reactive power optimization curve at node 24.

17:25, and 18:40 are four, six, and eight, respectively. The reactive power available for the grid configuration increases proportionally with an increase in the number of inverters in the free state. The available capacity curve for the third-tier reactive power optimization in Fig. 8 shows that as the PV output decreases, the remaining capacity of the PV cluster control system and power available for third-tier reactive power optimization increase. By contrast, the power available for third-tier reactive power optimization becomes 0 or the maximum output value when the PV output increases or decreases to a certain value.

Fig. 9 shows the power output curves of the reactive power compensation equipment at each response level on node 24, and Table 6 presents the voltage of this node during the 18th and 19th periods. It can be seen from Fig. 9 that the SCB is involved in the first layer of reactive power optimization with an hourly response period. In the PV cluster control system, the PV inverters use GFL control and participate in the second layer of reactive power optimization with the same response period as the centralized regulation command. Additionally, the frame network control of the PV inverted participates in the third layer of reactive power optimization and can respond in real time. As the time window is 5 min, optimizations are performed every 5 min. The inverter's frame network control does not participate in reactive power optimization at the moment when the centralized regulation command is executed. Therefore, this study provides an auxiliary reactive power compensation capacity, thereby reducing the cost of the dedicated equipment configuration and improving the system voltage level.

TABLE 6. Voltage distribution characteristics before and after optimizing configuration at node 24.

Strategy	Voltage deviation		
	Maximum (%)	Minimum (%)	Average (%)
Before allocation	6.14	3.21	4.73
Proposed strategy	4.18	2.39	3.24
Ref. [24], [25]	4.36	3.02	3.69
Ref. [21]	5.61	3.66	4.54

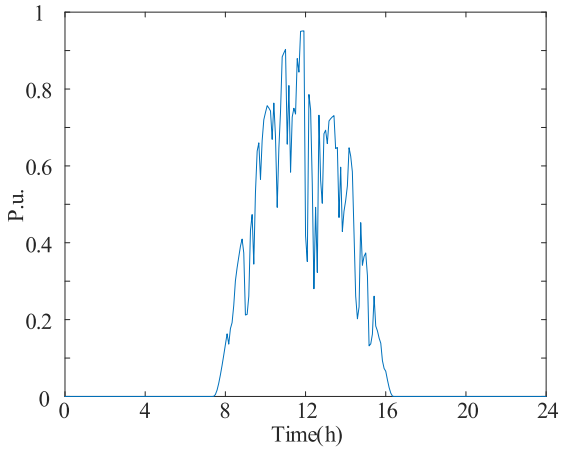

FIGURE 10. 24-h PV generation output curve.

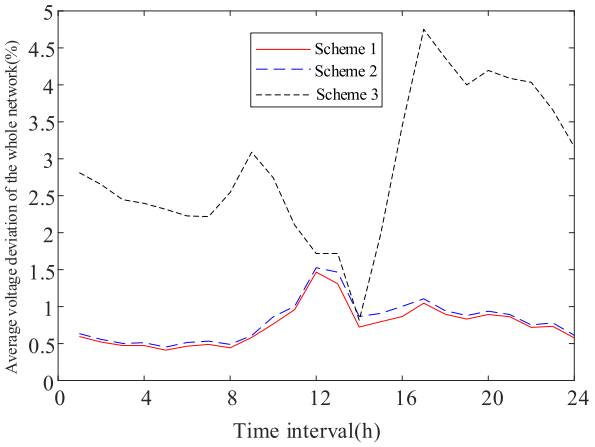

FIGURE 11. Average voltage deviation curve for each period in the IEEE 33-node system.

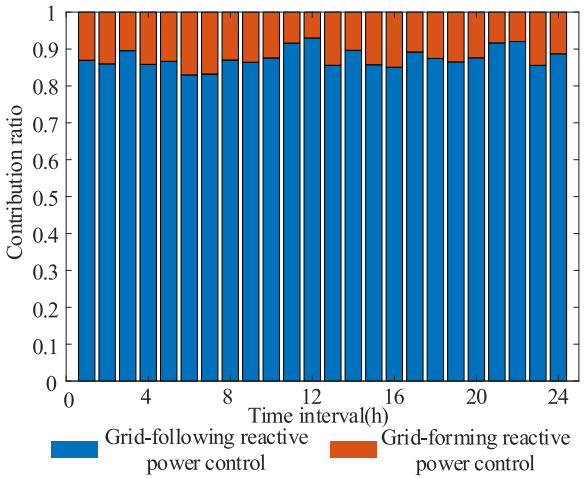

FIGURE 12. Ratio of the reactive power output contribution of the grid-forming (GFM) and grid-following (GFL) equipment in each period in the IEEE 33-node system.

Table 6 shows the characteristics of the voltage distribution of node 24 before and after the optimal configuration in the 18th and 19th periods. The node voltage reaches a maximum of 6.14% (which exceeds the 5% criterion) and substantially decreases after the optimal configuration of the reactive power. As outlined in Table 6, the configuration of the configuration network control function for the power electronic equipment was not considered in previous studies [21], [24], [25]. Moreover, the capacity of the configuration network control in such studies is insufficient for voltage optimization, and the maximum, minimum, and average values of the voltage deviations are worse than those obtained in this study. This shows that the proposed strategy is better than those mentioned above.

3) ANALYSIS OF OPTIMIZATION RESULTS OF FULL-DAY RUNNING SCENARIO AFTER CONFIGURATION

A typical load curve was retained; then, the entire day average voltage of the entire network after configuration was analyzed based on a randomly-selected day during the entire PV output operation scenario. Fig. 10 shows the PV power output curve, where the quasi-value of the vertical coordinate is based on the rated output power of a single inverter.

The analysis of the average voltage and power of the reactive equipment during each period shows that the three scenarios defined in this section are comparable under the same optimized configuration. Fig. 11 shows the average voltage deviation curve for the entire network at each time after the optimized configuration. The voltage deviation of the entire network fluctuates more in Scheme 3, mainly owing to the influence of the fluctuation in the PV output. The insufficient and adjustable amount of reactive power involved in the optimization results in the worst voltage operation level for the entire network. In Scheme 2, the active-reactive power compensation function of the power electronic inverter is not considered. However, a more significant improvement is observed relative to that of Scheme 1. Moreover, the performance advantages of each equipment in Scheme 1 are fully exploited and the average voltage deviation in the entire network is smaller each time compared with those of other schemes. This further reflects the effectiveness of the proposed synergistic optimization configuration strategy.

The first and second layers of the reactive power optimization are then used for the optimization results for the following network equipment. The third layer of reactive power optimization is used for the optimization results for the GFM equipment. According to the reactive power optimization of the operation scenario, the contribution ratio of the optimization of the GFM and GFL reactive power equipment at each time is shown in Fig. 12 for the entire network. It shows that the power electronic equipment still has the advantage of network optimization based on the reactive power optimization, which can enhance the grid voltage operation level. To reach the required confidence level for the optimal configuration, the configuration-network-type equipment are configured using a lower capacity. The remaining capacity of the configuration-network-type equipment is used

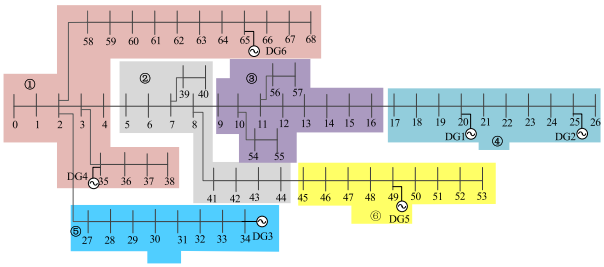

FIGURE 13. Division of the reactive power area in the IEEE 69-node system.

TABLE 7. PV configuration information of the IEEE 69-Node system.

Access location	20	25	34	35	49	65
Number of PV inverters	24	24	24	16	24	16

for reactive power optimization within the network. This shows that to achieve an optimal configuration confidence level, a low-GFM equipment should be employed, and the remaining capacity of the GFM equipment should be used to follow the grid reactive power optimization. It is possible to participate in the following grid reactive power optimization for a certain period. Moreover, by combining the average voltage deviation in the grid at each time period in the three scenarios in Fig. 12, it can be seen that the proposed strategy fully exploits the functional advantages of the reactive power equipment without increasing the equipment cost. This improves the voltage operation level of the entire network and further reflects the effectiveness of the proposed strategy.

VI. CASE STUDY ON IEEE 69-NODE SYSTEM

The IEEE 69-node system with some distributed PVs is used for investigating the effectiveness of the proposed method. In this case, only certain important results and analyses are provided. The partitioning results are shown in Fig. 13 [19] and the configuration information for the PV is presented in Table 7. The strategies for the three schemes are the same as those in the IEEE 33-node system case study. The configuration results for the IEEE 69-node system are shown in Table 8. Owing to the voltage constraints being satisfied by all nodes in Zone ①, no reactive power equipment is configured in this zone.

The configuration information of Scheme 1 is used for a comparative analysis of the simulation results from all three schemes. The average voltage deviation curves of the entire network after optimization are depicted in Fig. 14. It shows that Scheme 1 exhibits smaller average voltage deviations than the other schemes across the different time periods.

The proposed strategy for reactive power optimization in operational scenarios is used to assess the optimization contributions of the GFL and GFM reactive power equipment in the IEEE 69-node system. This assessment is conducted across different time periods and the results are illustrated in Fig. 15. The figure reveals the active participation of the GFM equipment in reactive power optimization throughout all time periods. Although their contribution to the overall reactive power control capacity is relatively small compared to that of the GFL equipment, the combination of observations from

TABLE 8. Optimal allocation results for special reactive power equipment.

Scheme	Equipment	Dominant nodes determined	Installed capacity (kvar)	Annual investment cost (thousand yuan)
1	SCB	/	/	16.0
	SVG	16, 25	300, 350	
2	SCB	/	/	25.9
	SVG	16，25	500，700	
3	SCB	51	150	36.7
	SVG	16，25，34，44，51	600，750，50，50，200	

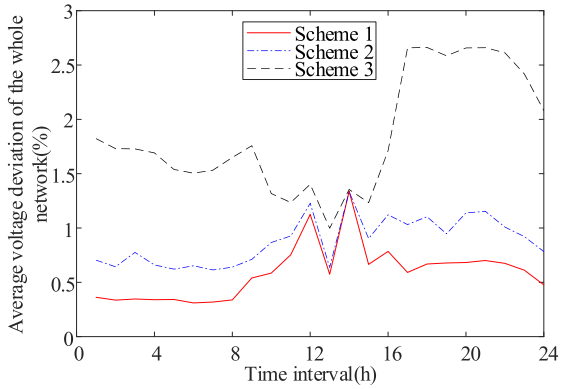

FIGURE 14. Division of the reactive power area in the IEEE 69-node system.

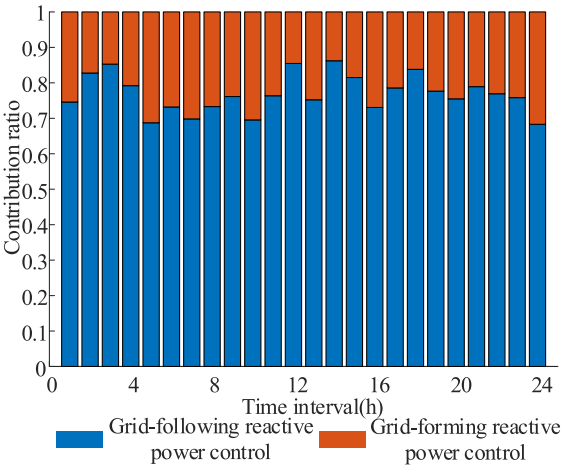

FIGURE 15. Ratio of the reactive power output contributions of the GFM and GFL equipment in each period in the IEEE 69-node system.

Fig. 14 highlights the effective utilization of the functional advantages of GFM equipment with the proposed strategy. This is achieved without requiring additional reactive power equipment. Consequently, an improved voltage operating level is achieved across the entire network, further reflecting the efficacy of the proposed strategy.

VII. CONCLUSION

In this study, a cooperative optimal allocation strategy for GFL and GFM reactive power resources was proposed based on distribution network partitioning and in consideration of the variability in the reactive power equipment costs and tracking response capabilities. A Markov chain-based source-load stochastic modeling method was used to construct an uncertain operation scenario for the distribution network. It was then used to solve the voltage-crossing limit problem to achieve the optimal allocation under the opportunity constraints. The number of free states of inverters in the different DPV cluster operation scenarios was then considered for the PV output analysis to provide an auxiliary reactive capacity for the GFM reactive equipment. Subsequently, a joint reactive power optimal allocation model was established using the primary and auxiliary decisions. The primary decision provided the equipment capacity for the auxiliary decision, and the auxiliary decision provided the equipment desired capacity for the primary decision, thereby minimizing the annual investment cost and voltage deviation. The simulation results showed that current power electronics can be used for network control reactive power optimization based on the following network control reactive power optimization. In addition, the active-reactive power compensation functions of the power electronics were analyzed to further enhance the reactive power equipment performance and alleviate short-time voltage fluctuations in the power grid. The auxiliary function for the network construction of the part-time equipment could further reduce the total investment cost and improve the level of the voltage deviation in the entire network. A comparative analysis of three schemes showed that the proposed strategy guaranteed lower overall network voltages while achieving cost reductions of at least 20% compared to those of other schemes. In addition, the configuration capacity of GFM equipment was typically small; thus, the residual capacity of the GFM equipment was only used for the reactive power optimization of the GFL equipment at certain times.

In the future, we will continue to explore how to enhance the performance synergies of power electronic equipment and improve various power quality problems.

DECLARATION OF COMPETING INTEREST

The authors declare that they have no known competing financial interests or personal relationships that could have appeared to influence their work. They also declare that they have no known competing financial interests or personal relationships that could have appeared to influence the work reported in this articles.

REFERENCES

[1] X. Yao, H. Lei, L. Yang, S. Shao, D. Ahmed, and M. G. A. Ismaail, "Low-carbon transformation of the regional electric power supply structure in China: A scenario analysis based on a bottom-up model with resource endowment constraints," *Resour., Conservation Recycling*, vol. 167, Apr. 2021, Art. no. 105315.

[2] S. Liu, Y. Jiang, S. Yu, W. Tan, T. Zhang, and Z. Lin, "Electric power supply structure transformation model of China for peaking carbon dioxide emissions and achieving carbon neutrality," *Energy Rep.*, vol. 8, pp. 541–548, Nov. 2022.

[3] J. O. Petinrin and M. Shaabanb, "Impact of renewable generation on voltage control in distribution systems," *Renew. Sustain. Energy Rev.*, vol. 65, pp. 770–783, Nov. 2016.

[4] M. Oshiro, K. Tanaka, A. Uehara, T. Senjyu, Y. Miyazato, A. Yona, and T. Funabashi, "Optimal voltage control in distribution systems with coordination of distribution installations," *Int. J. Electr. Power Energy Syst.*, vol. 32, no. 10, pp. 1125–1134, Dec. 2010.

[5] V. B. Pamshetti, S. Singh, A. K. Thakur, and S. P. Singh, "Multistage coordination Volt/VAR control with CVR in active distribution network in presence of inverter-based DG units and soft open points," *IEEE Trans. Ind. Appl.*, vol. 57, no. 3, pp. 2035–2047, May 2021.

[6] R. Sirjani and A. R. Jordehi, "Optimal placement and sizing of distribution static compensator (D-STATCOM) in electric distribution networks: A review," *Renew. Sustain. Energy Rev.*, vol. 77, pp. 688–694, Sep. 2017.

[7] B. Ismail, N. I. A. Wahab, M. L. Othman, M. A. M. Radzi, K. N. Vijyakumar, and M. N. M. Naain, "A comprehensive review on optimal location and sizing of reactive power compensation using hybrid-based approaches for power loss reduction, voltage stability improvement, voltage profile enhancement and loadability enhancement," *IEEE Access*, vol. 8, pp. 222733–222765, 2020.

[8] Q. Nguyen, X. Ke, N. Samaan, J. Holzer, M. Elizondo, H. Zhou, Z. Hou, R. Huang, M. Vallem, B. Vyakaranam, M. Ghosal, and Y. V. Makarov, "Transmission-distribution long-term Volt-VAR planning considering reactive power support capability of distributed PV," *Int. J. Electr. Power Energy Syst.*, vol. 138, Jun. 2022, Art. no. 107955.

[9] V. B. Pamshetti and S. P. Singh, "Optimal coordination of PV smart inverter and traditional Volt-VAR control devices for energy cost savings and voltage regulation," *Int. Trans. Electr. Energy Syst.*, vol. 29, no. 7, pp. 1–24, Jun. 2019.

[10] S. Singh, V. B. Pamshetti, A. K. Thakur, and S. P. Singh, "Multistage multiobjective Volt/VAR control for smart grid-enabled CVR with solar PV penetration," *IEEE Syst. J.*, vol. 15, no. 2, pp. 2767–2778, Jun. 2021.

[11] N. H. Khan, Y. Wang, D. Tian, R. Jamal, S. Kamel, and M. Ebeed, "Optimal siting and sizing of SSSC using modified salp swarm algorithm considering optimal reactive power dispatch problem," *IEEE Access*, vol. 9, pp. 49249–49266, 2021.

[12] M. Ćalasan, T. Konjić, K. Kecojević, and L. Nikitović, "Optimal allocation of static Var compensators in electric power systems," *Energies*, vol. 13, no. 12, p. 3219, Jun. 2020.

[13] T. Zhang, X. Xu, Z. Li, A. Abu-Siada, and Y. Guo, "Optimum location and parameter setting of STATCOM based on improved differential evolution harmony search algorithm," *IEEE Access*, vol. 8, pp. 87810–87819, 2020.

[14] Z. Deng, M. Liu, Y. Ouyang, S. Lin, and M. Xie, "Multi-objective mixed-integer dynamic optimization method applied to optimal allocation of dynamic Var sources of power systems," *IEEE Trans. Power Syst.*, vol. 33, no. 2, pp. 1683–1697, Mar. 2018.

[15] Y. Liu, X.-Y. Xiao, X.-P. Zhang, and Y. Wang, "Multi-objective optimal STATCOM allocation for voltage sag mitigation," *IEEE Trans. Power Del.*, vol. 35, no. 3, pp. 1410–1422, Jun. 2020.

[16] A. Noori, Y. Zhang, N. Nouri, and M. Hajivand, "Multi-objective optimal placement and sizing of distribution static compensator in radial distribution networks with variable residential, commercial and industrial demands considering reliability," *IEEE Access*, vol. 9, pp. 46911–46926, 2021.

[17] M. El-Azab, W. A. Omran, S. F. Mekhamer, and H. E. A. Talaat, "Allocation of FACTS devices using a probabilistic multi-objective approach incorporating various sources of uncertainty and dynamic line rating," *IEEE Access*, vol. 8, pp. 167647–167664, 2020.

[18] A. A. Shehata, M. A. Tolba, A. M. El-Rifaie, and N. V. Korovkin, "Power system operation enhancement using a new hybrid methodology for optimal allocation of FACTS devices," *Energy Rep.*, vol. 8, pp. 217–238, Nov. 2022.

[19] S. Tian, Q. Jia, S. Xue, H. Yu, Z. Qu, and T. Gu, "Collaborative optimization allocation of VDAPFs and SVGs for simultaneous mitigation of voltage harmonic and deviation in distribution networks," *Int. J. Electr. Power Energy Syst.*, vol. 120, Sep. 2020, Art. no. 106034.

[20] A. Noori, Y. Zhang, N. Nouri, and M. Hajivand, "Hybrid allocation of capacitor and distributed static compensator in radial distribution networks using multi-objective improved golden ratio optimization based on fuzzy decision making," *IEEE Access*, vol. 8, pp. 162180–162195, 2020.

[21] A. A. Abou El-Ela, R. A. El-Sehiemy, A. M. Shaheen, and I. A. Eissa, "Optimal coordination of static var compensators, fixed capacitors, and distributed energy resources in Egyptian distribution networks," *Int. Trans. Electr. Energy Syst.*, vol. 30, no. 11, pp. 1–26, Sep. 2020.

[22] K. Mahmoud and M. Lehtonen, "Simultaneous allocation of multi-type distributed generations and capacitors using generic analytical expressions," *IEEE Access*, vol. 7, pp. 182701–182710, 2019.

[23] H. Lotfi, "Optimal sizing of distributed generation units and shunt capacitors in the distribution system considering uncertainty resources by the modified evolutionary algorithm," *J. Ambient Intell. Humanized Comput.*, vol. 13, no. 10, pp. 4739–4758, Oct. 2022.

[24] H. Pezeshki, A. Arefi, G. Ledwich, and P. Wolfs, "Probabilistic voltage management using OLTC and dSTATCOM in distribution networks," *IEEE Trans. Power Del.*, vol. 33, no. 2, pp. 570–580, Apr. 2018.

[25] S. Tian, Q. Jia, Y. Cui, S. Xue, H. Yu, and W. Liu, "Multi-objective collaborative optimization of VDAPFs and SVGs allocation considering MFGCIs contribution for voltage partitioning mitigation in distribution networks," *Electr. Power Syst. Res.*, vol. 207, Jun. 2022, Art. no. 107830.

[26] Q. Zhang, F. Bu, Y. Guo, and Z. Wang, "Tractable data enriched distributionally robust chance-constrained conservation voltage reduction," *IEEE Trans. Power Syst.*, early access, Feb. 14, 2023, doi: 10.1109/TPWRS.2023.3244895.

[27] A. Zhou, H. Zhai, M. Yang, and Y. Lin, "Three-phase unbalanced distribution network dynamic reconfiguration: A distributionally robust approach," *IEEE Trans. Smart Grid*, vol. 13, no. 3, pp. 2063–2074, May 2022.

[28] S. Xue, Q. Jia, K. Zhang, Z. Gao, J. Liang, and Y. Li, "Electricity-consumption-data-driven stochastic modeling and unbalance assessment of load in low-voltage distribution network," *Autom. Electr. Power Syst.*, vol. 46, no. 8, pp. 143–153, Apr. 2022.

[29] R. Besharati, M. H. Rezvani, and M. M. G. Sadeghi, "An auction-based bid prediction mechanism for fog-cloud offloading using Q-learning," *Complexity*, vol. 2023, pp. 1–20, Jan. 2023.

[30] M. Naghdehforoushha, M. D. T. Fooladi, M. H. Rezvani, and M. M. G. Sadeghi, "BLMDP: A new bi-level Markov decision process approach to joint bidding andtask-scheduling in cloud spot market," *Turkish J. Electr. Eng. Comput. Sci.*, vol. 30, no. 4, pp. 1419–1438, May 2022.

[31] M. Gilvanejad, H. A. Abyaneh, and K. Mazlumi, "Estimation of the overload-related outages in distribution networks considering the random nature of the electrical loads," *IET Gener., Transmiss. Distrib.*, vol. 7, no. 8, pp. 855–865, Aug. 2013.

[32] X. Chen, T. Wei, and S. Hu, "Uncertainty-aware household appliance scheduling considering dynamic electricity pricing in smart home," *IEEE Trans. Smart Grid*, vol. 4, no. 2, pp. 932–941, Jun. 2013.

[33] F. J. Ruiz-Rodriguez, J. C. Hernández, and F. Jurado, "Voltage unbalance assessment in secondary radial distribution networks with single-phase photovoltaic systems," *Int. J. Electr. Power Energy Syst.*, vol. 64, pp. 646–654, Jan. 2015.

[34] J. Liu, Y. Miura, and T. Ise, "Comparison of dynamic characteristics between virtual synchronous generator and droop control in inverter-based distributed generators," *IEEE Trans. Power Electron.*, vol. 31, no. 5, pp. 3600–3611, May 2016.

[35] S. Xue, Q. Jia, S. Tian, Y. Su, and H. Yu, "Performance improvement strategy for photovoltaic generation through dynamic reconfiguration of cell strings," *Int. J. Electr. Power Energy Syst.*, vol. 125, Feb. 2021, Art. no. 106456.

[36] Z. Zhao, Z. Xu, J. Guo, P. Yang, and L. L. Lai, "Multi-time scale regional autonomous operation strategy for multi-microgrids with three-phase/single-phase hybrid structure," *IEEE Access*, vol. 8, pp. 85923–85938, 2020.

[37] Y. Guangyou, "A modified particle swarm optimizer algorithm," in *Proc. 8th Int. Conf. Electron. Meas. Instrum.*, Aug. 2007, pp. 2675–2679.

[38] Y.-K. Wu, C.-Y. Lee, L.-C. Liu, and S.-H. Tsai, "Study of reconfiguration for the distribution system with distributed generators," *IEEE Trans. Power Del.*, vol. 25, no. 3, pp. 1678–1685, Jul. 2010.

[39] R. Sirjani, A. Mohamed, and H. Shareef, "Optimal allocation of shunt Var compensators in power systems using a novel global harmony search algorithm," *Int. J. Electr. Power Energy Syst.*, vol. 43, no. 1, pp. 562–572, Dec. 2012.

SHIWEI XUE received the Ph.D. degree in power systems and its automation from Yanshan University, Qihuangdao, China, in 2022. He is currently a Researcher at the Postdoctoral Research Station jointly trained by the Electric Power Research Institute, State Grid Hebei Electric Power Company Ltd., and the School of Electrical Engineering, Yanshan University. His current research interests include optimal reactive power allocation and distributed resources coordinated control.

SIMING ZENG received the B.S. degree in industrial electric automation from the Hebei University of Technology, Tianjin, China, in 1991, and the M.S. degree in industrial engineering from North China Electric Power University, Beijing, China, in 2012. He is currently a Senior Engineer with the State Grid Hebei Electric Power Research Institute, Shijiazhuang, China. His current research interests include power information physical systems, active distribution network operation control, new energy active support, and dispatching control.

QINGQUAN JIA was born in Jilin, China, in January 1970. He received the Ph.D. degree from North China Electric Power University, China, in 2002. He is currently a Professor with Yanshan University. His current research interests include signal processing and fault diagnosis for power systems, power quality monitoring and control, distributed generation, and microgrids.

XUEKAI HU received the bachelor's and master's degrees in electrical engineering from the School of Electrical Engineering, Xi'an Jiaotong University, in 2009 and 2012, respectively. He is currently a Senior Engineer with the State Grid Hebei Electric Power Research Institute. His current research interests include electricity market operation and energy sharing.

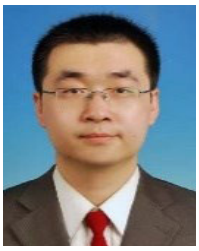

PENG LUO received the Ph.D. degree from Tianjin University, China, in 2012. He is currently with the State Grid Hebei Electric Power Research Institute. His current research interests include power system automation, new energy power systems, and intelligent power distribution technology.

JIFENG LIANG was born in Handan, China, in April 1985. He received the M.S. degree from North China Electric Power University. He is currently a Senior Engineer with the State Grid Hebei Electric Power Research Institute, Shijiazhuang, China. His current research interests include power system security analysis and new energy technology research.

LEI WANG received the M.S. degree from North China Electric Power University, China, in 2011. He is currently a Senior Engineer with the State Grid Hebei Electric Power Research Institute, Shijiazhuang, China. His current research interests include new energy technology and power quality.

WEN ZHOU received the M.S. degree from the State Grid Hebei Electric Power Research Institute. He was a Senior Professor Engineer with the State Grid Hebei Electric Power Research Institute. His current research interests include power system analysis and control, power quality analysis and management, and new energy grid technology research.